Cross-phase modulation and entanglement in a compound gradient echo memory

Shuangshuang Fu, André R. R. Carvalho, Michael R. Hush, and Matthew R. James

Phys. Rev. A **93**, 023809 — Published 4 February 2016

DOI: 10.1103/PhysRevA.93.023809

Cross phase modulation and entanglement in a compound gradient echo memory

Shuangshuang Fu,[1,2] André R. R. Carvalho,[3,4] Michael R. Hush,[5] and Matthew R. James[2,4]

[1] *School of Mathematics and Physics, University of Science and Technology Beijing, Beijing 100083, PR China*
[2] *Research School of Engineering, The Australian National University, Canberra, ACT 0200, Australia*
[3] *Department of Quantum Science, Research School of Physics and Engineering, Australian National University, Canberra, Australia*
[4] *ARC Centre for Quantum Computation and Communication Technology, The Australian National University, ACT 0200, Australia*
[5] *School of Engineering and Information Technology, University of New South Wales at ADFA, Canberra, ACT 2600, Australia*

We present a theoretical model for a Kerr-like interaction between two registers of a compound gradient echo memory (GEM). This type of interaction is known to generate cross-phase modulation (XPM) between optical fields, an effect that is limited by the typically small values of non-linearities in crystals. Here we show that in GEM systems the phase shift increases linearly with the interaction time and quadratically with the strength of the field. Increasing storage (interaction) times would then lead to stronger XPM effects even with fields with very low intensity. This interaction also generates two other effects: entanglement between the registers, which depends on the strength of the interaction and its spatial profile, and an interaction-induced gradient. We show that the later produces leakage during the storage stage depending on the shape of the stored pulses, an undesirable consequence that can be minimised by carefully designing the temporal profile of the input fields.

PACS numbers: 42.50.Gy 42.65.-k

I. INTRODUCTION

Photons are ideal carriers of quantum information due to their high speed and weak interactions with the environment. Proposals [1, 2] have been made to use photons as qubits in all-optical quantum computers. So-called deterministic protocols for computation require controllable interactions between photons, typically achieved using some mediating crystal or atomic vapor. The current limiting factor for these proposals has been generating interactions of sufficient strength [3, 4]. In particular, the deterministic scheme of Chuang and Yamamoto [5] is achieved via cross-phase modulation (XPM) induced by a cross-Kerr effect. There have been proposals on using optical fibres [6] or EIT like effects in atomic vapours [7] to achieve XPM, and much discussion on the viability of these approaches [8–11]. Recently, a XPM proof of principle experiment was performed in a Gradient Echo Memory (GEMs) where the interaction was produced using the AC-Stark effect [13]. The key to this demonstrations success was recognising large phase shifts can still be achieved with moderate interaction strengths as long as the interaction time can be made long. GEM have experimentally demonstrated long storage times with little loss; this makes them the ideal platform for performing XPM investigations.

We theoretically analyse a GEM with a generic Kerr nonlinearity. We include a kernel for our nonlinearity which can be local or non-local. Local interactions could be achieved with the AC-stark effect discussed in [13], while non-local interactions could be achieved using a Rydberg-state mediated interaction as described in [26]. By using a generic model we are able to determine what advantages or disadvantages different realizations of the nonlinearity may possess. We determine the scaling of the XPM as a function of the storage bandwidth and investigate the effects of a nonlocal interaction kernel. We furthermore investigate the presence of spatial entanglement in the memory due to the interactions. Lastly we discuss a problem we observed while performing XPM with a GEM, namely the presence of interaction-induced gradients that can lead to unwanted loss. We discuss potential ways to ameliorate these issues.

Our model is based on an input-output approach [16] derived in [15]. It is equivalent to the Maxwell-Bloch equations [12] which have also been used to analyse GEMs. We divide the whole process into three stages: write, interaction, and read. The write and read stages are described by quadratic Hamiltonians and can be solved exactly. However the interaction stage involves nonlinear quantum Langevin equations that must be approximated. We use a Gaussian approximation, which reduces the problem to a set of numerically solvable partial differential equations and allows for the use of convenient measures of entanglement like logarithmic negativity.

The paper is organized as follows: In Section II we describe our model, derive the dynamical equations and discuss the numerical approach. In Section III we analyse some interesting phenomena induced by the Kerr-like interaction. First, we discuss the creation and propagation of entanglement between the memories in Sec. III A. Second, we determine the scaling of the XPM with different physical parameters in Section III B. In particular, the results of this Section reveal that the phase shift of the Gaussian-shape pulse is proportional to the strength and duration of the other pulse. We also show, for the same maximum value of the interaction, that nonlocal profiles induce larger phase shift in the XPM as com-

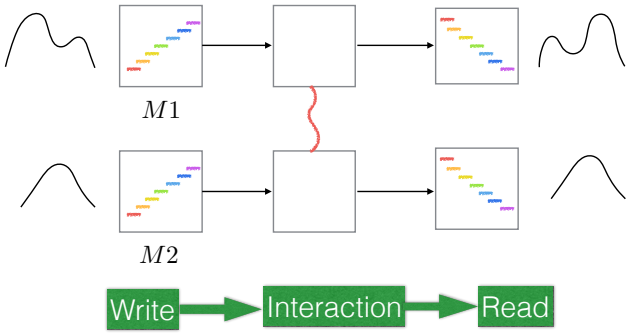

FIG. 1. In the write stage, the gradient is turned on and the two memory components $M1$ and $M2$ store the input pulses $b_{1,\mathrm{in}}(t)$ and $b_{2,\mathrm{in}}(t)$, respectively. After storage, the gradient is turned off and the interaction is turned on. Finally the gradient is flipped and the output pulses $b_{1,\mathrm{out}}(t)$ and $b_{2,\mathrm{out}}(t)$ are retrieved.

pared to local ones. Lastly, in Section III C, we discuss how the interactions can act like a gradient, which affects the storage. Details of the Gaussian approximation and calculations of the energy balance are presented in the Appendices.

II. MODEL OF THE INTERACTING COMPOUND GEM

A. Overview of the memory stages

Our model involves a memory consisting of two components, denoted by $M1$ and $M2$, as illustrated in Figure 1. Physically, these components could correspond to atomic ensembles, where different pulses are stored either in different atoms or into different atomic spin coherences as in [13]. The whole process can be described by the three stages shown in Figure 1:

- The write stage: The gradient is initially turned on and during the time interval $[0, t_1]$ the information contained in two independent input fields $b_{1,\mathrm{in}}(t)$ and $b_{2,\mathrm{in}}(t)$ are stored into $M1$ and $M2$, respectively.

- The interaction stage: In the interval $[t_1, t_2]$ the gradient is turned off and the two registers interact with each other through a Kerr-like interaction Hamiltonian.

- The read stage: during the interval $[t_2, t_3]$ the interaction is turned off and the gradient of each memory is flipped. Two output fields $b_{1,\mathrm{out}}(t)$ and $b_{2,\mathrm{out}}(t)$ are then retrieved.

B. Mathematical description of individual stages

We will now present the theoretical modelling for the three memory stages described above using the approach developed in [15]. First of all, for completeness, let us introduce some basic notations regarding the input-output model and algebraic descriptions of quantum networks of open quantum systems necessary to describe our system.

An open quantum system can be characterized by the parameter list $G = (S, L, H)$ [17], where S is the matrix describing the scattering of the bosonic field over different channels, L is the coupling operator to the environment, and H is the Hamiltonian of the system. For systems where there is no scattering of the bosonic field (as will be the case for our compound GEM) the operator S will be the identity and the system can be described by the parameters $G = (I, L, H)$. In this case, the quantum Langevin equation for an arbitrary operator X can be written as

$$\begin{aligned}\partial_t X = &-i[X, H] + \frac{1}{2}(L^\dagger[X, L] - [X, L^\dagger]L) \\ &+ b_{\mathrm{in}}^\dagger(t)[X, L] - [X, L^\dagger]b_{\mathrm{in}}(t),\end{aligned} \tag{1}$$

where $b_{\mathrm{in}}(t)$ is the input field driving the system. The corresponding output field is given by [16]

$$b_{\mathrm{out}}(t) = L(t) + b_{\mathrm{in}}(t). \tag{2}$$

In [15], this formalism was used to derive a GEM model as the continuum limit of a cascade network of oscillators. Since in the write and read stages our memory components $M1$ and $M2$ are decoupled, we can simply use the results from [15] to describe them. Both stages can be written in the same form, with the triple $G_j = (I, L_j, H_j)$ for the memory component j given by

$$L_j = \int_{-\eta}^{\eta} d\xi\, i\sqrt{\beta} a_j(\xi, t), \tag{3}$$

$$\begin{aligned}H_j = &\pm \int_{-\eta}^{\eta} d\xi\, \xi a_j^\dagger(\xi, t) a_j(\xi, t) \\ &+ \frac{\beta}{2i} \int_{-\eta}^{\eta} d\xi \int_{-\eta}^{\xi} d\xi' \left(a_j^\dagger(\xi, t) a_j(\xi', t) - a_j^\dagger(\xi', t) a_j(\xi, t) \right).\end{aligned} \tag{4}$$

Here $a_j(\xi)$ is the annihilation operator satisfying $[a_j(\xi), a_i^\dagger(\xi')] = \delta_{ij}\delta(\xi - \xi')$, β is the coupling coefficient of the oscillators with the bath (assumed to be the same for both components), and $[-\eta, \eta]$ is the frequency bandwidth of the memory. The sign of the first term in the Hamiltonian depends on the gradient, being positive for the write stage and negative for the read stage.

When describing open quantum systems connected in a quantum network, we employ the algebraic tools introduced in [17]. For the compound GEM model depicted in Fig. 2, we have two open quantum systems given by

$G_1 = (I, L_1, H_1)$ and $G_2 = (I, L_2, H_2)$. Their concatenation is denoted as $G_1 \boxplus G_2$ with parameters given by

$$G_1 \boxplus G_2 = \left(\begin{pmatrix} I & 0 \\ 0 & I \end{pmatrix}, \begin{pmatrix} L_1 \\ L_2 \end{pmatrix}, H_1 + H_2 \right). \quad (5)$$

For the write and read stages L_j and H_j are simply given by Eqs.(3) and (4). In the interaction phase, the Hamiltonian for the compound system can be expressed as

$$H(t) = H_1(t) + H_2(t) + H_{\text{xpm}}(t),$$

where

$$H_{\text{xpm}}(t) = \int_{-\eta}^{\eta}\int_{-\eta}^{\eta} d\xi_1 d\xi_2 \chi(\xi_1, \xi_2, t) a_1^\dagger(\xi_1, t) a_1(\xi_1, t) a_2^\dagger(\xi_2, t) a_2(\xi_2, t)$$

represents the Kerr-like Hamiltonian for the interacting memories. The entire process can then be described by the parameters $G = (I, L, H(t))$, with $L = \begin{pmatrix} L_1 \\ L_2 \end{pmatrix}$, and $H(t)$ given as follows:

$$\begin{aligned} H(t) &= \int_{-\eta}^{\eta} d\xi g(\xi, t)(a_1^\dagger(\xi, t) a_1(\xi, t) + a_2^\dagger(\xi, t) a_2(\xi, t)) \\ &+ \int_{-\eta}^{\eta}\int_{-\eta}^{\eta} d\xi_1 d\xi_2 \chi(\xi_1, \xi_2, t) a_1^\dagger(\xi_1, t) a_1(\xi_1, t) a_2^\dagger(\xi_2, t) a_2(\xi_2, t) \\ &+ \frac{\beta}{2i}\int_{-\eta}^{\eta} d\xi \int_{-\eta}^{\xi} d\xi' \left(a_1^\dagger(\xi, t) a_1(\xi', t) - a_1^\dagger(\xi', t) a_1(\xi, t) \right) \\ &+ \frac{\beta}{2i}\int_{-\eta}^{\eta} d\xi \int_{-\eta}^{\xi} d\xi' \left(a_2^\dagger(\xi, t) a_2(\xi', t) - a_2^\dagger(\xi', t) a_2(\xi, t) \right). \end{aligned} \quad (6)$$

The different stages of the process can be included under the same form by defining the time-dependent gradient

$$g(\xi, t) = \begin{cases} \xi, & t \in [0, t_1] \\ 0, & t \in (t_1, t_2) \\ -\xi, & t \in [t_2, t_3] \end{cases} \quad (7)$$

and Kerr-coefficient

$$\chi(\xi_1, \xi_2, t) = \begin{cases} 0, & t \in [0, t_1] \\ A \exp\left(-K(\xi_1 - \xi_2)^2\right), & t \in (t_1, t_2) \\ 0, & t \in [t_2, t_3] \end{cases} \quad (8)$$

where A represents the maximum strength of the interaction and K determines the spatial range of the interaction. With current experiments the most likely candidate to create such non-local interaction would be a Rydberg system. Using the off-resonant Rydberg states similar to that in Ref. [26], the effective interaction distance can be tuned using a combination of the detuning and the orbital number of the particular Rydberg state targeted. From Eq. (8), we can see that as K increases, the interaction becomes more localized in the sense that only when $|\xi_1 - \xi_2|$ is small enough can mode $a_1(\xi_1, t)$ interact with mode $a_2(\xi_2, t)$. We discuss this in detail in Section III B 3.

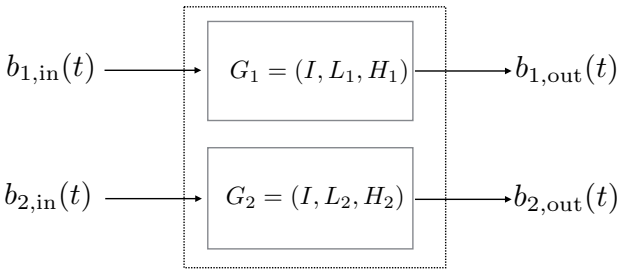

FIG. 2. Schematics of the compound GEM. The model corresponds to the concatenation of the two memory components given by G_1 and G_2.

C. Dynamical Equations

Given the triple $G = (I, L, H(t))$, we can employ the quantum Langevin equation (1) and the input-output equation (2) to derive the following equations for the whole process:

$$\begin{aligned} \partial_t a_1(\xi, t) &= -ig(\xi, t) a_1(\xi, t) - \beta \int_{-\eta}^{\xi} d\xi' a_1(\xi', t) \\ &\quad - i\int_{-\eta}^{\eta} d\xi' \chi(\xi, \xi', t) a_2^\dagger(\xi', t) a_2(\xi', t) a_1(\xi, t) \\ &\quad + i\sqrt{\beta} b_{1,in}(t) \end{aligned} \quad (9)$$

$$b_{1,\text{out}}(t) = i\sqrt{\beta}\int_{-\eta}^{\eta} d\xi a_1(\xi, t) + b_{1,\text{in}}(t), \quad (10)$$

$$\begin{aligned} \partial_t a_2(\xi, t) &= -ig(\xi, t) a_2(\xi, t) - \beta \int_{-\eta}^{\xi} d\xi' a_2(\xi', t) \\ &\quad - i\int_{-\eta}^{\eta} d\xi' \chi(\xi', \xi, t) a_1^\dagger(\xi', t) a_1(\xi', t) a_2(\xi, t) \\ &\quad + i\sqrt{\beta} b_{2,in}(t) \end{aligned} \quad (11)$$

$$b_{2,\text{out}}(t) = i\sqrt{\beta}\int_{-\eta}^{\eta} d\xi a_2(\xi, t) + b_{2,\text{in}}(t), \quad (12)$$

where $b_{i,\text{in}}(t) (i = 1, 2)$ are the input light fields for the two registers.

Note that these Langevin equations are identical to the model of a GEM using the Maxwell-Bloch equations [12]. The a_1 and a_2 operators physically correspond to the coherence of the atomic ensemble. The $b_{1,\text{out}}(t)$ and $b_{2,\text{out}}(t)$ operators correspond to the strength of the electric-magnetic field at the end of the memory. Hence our model includes coupling between the atomic ensemble and the light field along the propagation direction of the GEM. Thus loss is included in our model due to spontaneous emission, but this is typically suppressed in the operation of a GEM due to destructive interference of the atomic coherence due to different rotating phases along the gradient. We do not include atomic dephasing due to diffusion, or spontaneous emission of light in directions perpendicular to the applied magnetic gradient.

The rates of these other processes are typically very small on the time scale of the GEMs operation [12].

D. Numerical model: Gaussian approximation

Note that the dynamical equations (9-12) are nonlinear. The equation for the expectation value $\langle a_1(\xi,t)\rangle$, for example, depends on $\langle a_1(\xi,t)a_2^\dagger(\xi,t)a_2(\xi,t)\rangle$, which depends on even higher-order terms. This generates an infinite number of coupled differential equations which not only prevents an analytical approach as done in [15], but requires some approximation for a numerical solution as well.

Our approach is to assume that the states of the oscillators representing the memories are Gaussian. This is a sort of a semiclassical approximation that allows us to write all higher order expectation values only in terms of first and second-order moments. This simplifies the problem which now requires the numerical solution of only 8 coupled equations. A detailed derivation of the remaining equations and the Gaussian approximation are presented in Appendix A.

In our simulations, done using the XMDS package [18], we consider coherent input fields with a Gaussian pulse shape for $M1$ and a rectangular pulse shape for $M2$, therefore the expectations of the two input fields read

$$\langle b_{1,\mathrm{in}}(t)\rangle = \begin{cases} \alpha_1(t), & t\in[0,t_1] \\ 0, & t\in(t_1,t_2) \\ 0, & t\in[t_2,t_3] \end{cases}$$

with $\alpha_1(t)$ being a Gaussian-shape pulse, and

$$\langle b_{2,\mathrm{in}}(t)\rangle = \begin{cases} \alpha, & t\in[0,t_1] \\ 0, & t\in(t_1,t_2) \\ 0, & t\in[t_2,t_3] \end{cases}$$

with α being a constant.

For these simulations, we express the parameters in terms of the memory bandwidth, a crucial property of the GEM determined by the value of η, and set all the parameters to be dimensionless. The pulse $\alpha_1(t)$, for example, is chosen so that its width in the frequency domain fits well within the memory bandwidth. Write, read, and interaction times are all set to $\tau = 100/\eta$, much longer than the pulse width in time. For the interaction term, we set $A/\eta = 0.005$ and $K\eta^2 = 10$. A is the smallest frequency of the problem, but still big enough for nonlinearity effects to be appreciable in the timescales of our simulations. The parameter $K\eta^2 = 10$ corresponds to a fairly nonlocal interaction, also chosen to highlight this effect. Note, however, that for the cross-phase modulation described in the next section, K is varied so that we can investigate the effect of the spatial extent of the interactions.

III. EFFECTS OF INTERACTION

In this section, we investigate three interesting and important phenomena generated under the dynamics, which are the entanglement formation, the cross-phase modulation and the interaction-induced gradient.

A. Entanglement between memory registers

Interactions can generate nonclassical correlations between two systems. It is interesting to look at the nonclassical correlations generated between the registers under the interaction Hamiltonian (Eq.(6) for $t \in (t_1, t_2)$). Although the interaction Hamiltonian is not quadratic in the canonical operators, which means we cannot guarantee that the state will remain Gaussian, we expect the approximation to be quantitatively valid for short interaction time and qualitatively informative for longer time. In the following, we employ Logarithmic negativity as a measure of entanglement for two-mode Gaussian states [21–23] and study the entanglement generated in the interaction stages. Recall that for a two-mode Gaussian state ρ_{AB}, Logarithmic negativity is a measure of entanglement based on the violation of the PPT (positive partial transpose) criterion. It is defined as $E_N(\rho_{AB}) := \log(\|\rho_{AB}^{T_A}\|)$ where $\|O\|$ is the trace distance, i.e. the sum of the absolute values of the operator O. $E_N(\rho_{AB})$ depends only on the symplectic eigenvalues $\tilde{v}_k$ of the partial transposed state $\rho_{AB}^{T_A}$ which can be smaller than 1. Explicitly

$$E_N(\rho_{AB}) = \begin{cases} 0, & \text{if } \tilde{v}_k \geq 1 \ \forall\ k, \\ -\sum_{\{k:\tilde{v}_k<1\}} \log \tilde{v}_k. \end{cases} \quad (13)$$

We study the entanglement generated between modes of different registers during the interaction phase. For mode $a_1(\xi_1,t)$ of $M1$ and mode $a_2(\xi_2,t)$ of $M2$, we numerically calculate the 4×4 covariance matrix $\sigma(\xi_1,\xi_2)$ and apply partial transposition to obtain $\tilde{\sigma}(\xi_1,\xi_2)$, from which we can further calculate the symplectic eigenvalues $\tilde{v}_k(\xi_1,\xi_2)$. The logarithmic negativity corresponding to the two mode state can be calculated by Eq.(13) and plotted in Figure 3 as a function of ξ_1 and ξ_2. We can see entanglement can be generated between different modes corresponding to different spatial variables. This is because the chosen value for K corresponds to a nonlinear interaction that spreads across most of the memory, letting modes $a_1(\xi_1,t)$ and $a_2(\xi_2,t)$ interact as long as $|\xi_1-\xi_2|$ is not too large.

B. Cross-phase modulation

In the experiment performed in [13], heterodyne detection was used to observe the phase shift. Mathematically, if we express the output pulse $b_{\mathrm{out}}(t)$ as $b_{\mathrm{out}}(t) =$

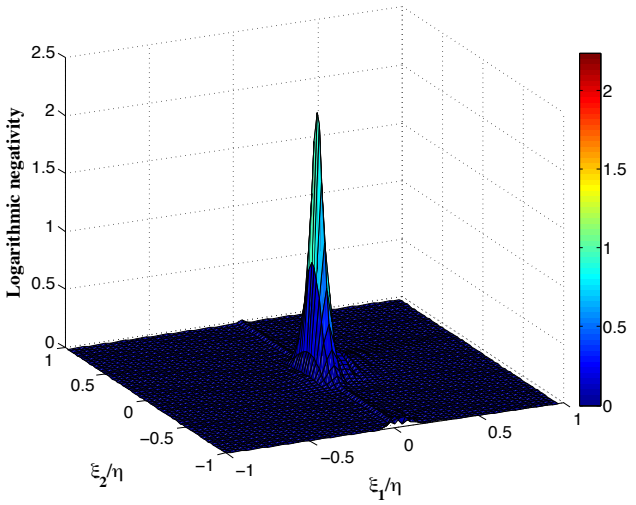

FIG. 3. Logarithmic negativity between two modes $a_1(\xi_1, t)$ and $a_2(\xi_2, t)$ near the end of the interaction stage ($t = 187.5/\eta$. ξ_i/η (i=1,2) are dimensionless parameters denoting two modes.

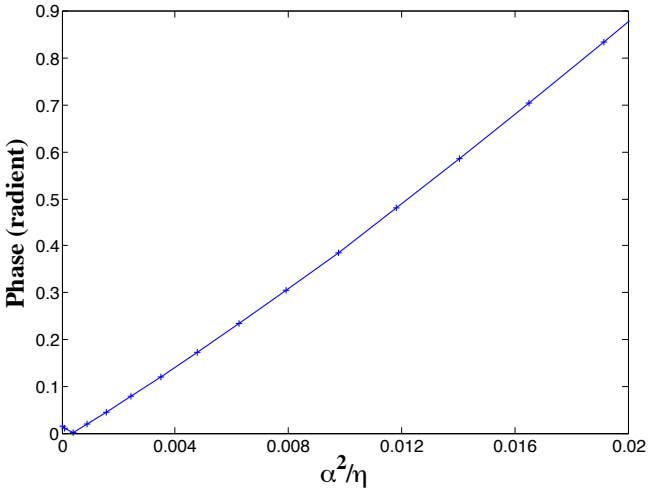

FIG. 4. Numerical results demonstrating the phase shift of the first output pulse as a quadratic function of the strength of the second pulse. Here '+' denotes the points calculated numerically, the solid line is the fitting curve obtained, and α^2/η is a dimensionless parameter quantifying the squared amplitude of the second pulse.

$\Re(b_{\text{out}}(t)) + i\Im(b_{\text{out}}(t)) = \|b_{\text{out}}(t)\|e^{i\theta(t)}$ and set the frequency of the local oscillator to be ω, then

$$\begin{aligned}
&\Re(b_{\text{out}}(t)e^{i\omega t}) \\
&= \Re(b_{\text{out}}(t))\cos(\omega t) - i\Im(b_{\text{out}}(t))\sin(\omega t) \\
&= \|b_{\text{out}}(t)\|\left(\frac{\Re(b_{\text{out}}(t))}{\|b_{\text{out}}(t)\|}\cos(\omega t) - \frac{\Im(b_{\text{out}}(t))}{\|b_{\text{out}}(t)\|\}}\sin(\omega t)\right) \\
&= \|b_{\text{out}}(t)\|\cos(\theta(t) + \omega t).
\end{aligned}$$

The phase shift can be calculated by looking into the fluctuation component of $\Re(b_{\text{out}}(t)e^{i\omega t})$ which is a cosine function. We can calculate the corresponding phase shift by comparing the cosine functions under different situations. Since the strength of the second pulse α and the interaction duration $\tau = t_2 - t_1$ are two key factors in the study of XPM [13], in the following subsections we set $\omega/\eta = 0.5$ and ran several simulations, mainly to investigate the dependence of the phase shift with respect to these two factors. Also we did a numerical investigation into the effect of local and nonlocal interactions in the XPM.

1. *Phase shift v.s. pulse strength*

We investigate the influence of the strength of the rectangular-shape pulse α on the phase of the first Gaussian-shape pulse by fixing the interaction duration. In our simulation we set $\tau = 100/\eta$, numerical results are given in Figure 4 which reveals that the phase shift will increase as α increases. Similar results have been demonstrated in previous work [13, 19].

2. *Phase shift v.s. interaction duration*

Now we fix the strength of the second input pulse to be $\alpha^2 = 0.025\eta$ and look into the dependence of the phase shift on the interaction duration τ. In Figure 5, we numerically calculate the phase shift as $\eta\tau$ increases from 10 to 100. We can observe an increase in the phase shift of the output pulse as τ grows. In practice, this phase shift increase would eventually stop when dephasing processes in the system become relevant. The quality of the quantum memory will determine the maximum phase shift that can be reliably produced.

3. *Phase shift v.s. local/nonlocal interactions*

The parameter K in Eq. (8) can be used to adjust the interaction range between the two registers. Larger K means narrower interaction range, which correspond to more local interactions, while smaller K means wider interaction range, which correspond to more nonlocal interaction. As has been demonstrated before, nonlocal interactions create entanglement between different modes. In the following, we numerically investigate the effect of local and nonlocal interactions on the phase shift. The numerical results are shown in Figure 6, from which we can infer that with the same maximum interaction value A, nonlocal interaction range would perform better compared to local interaction range in the sense that the induced phase shift is larger.

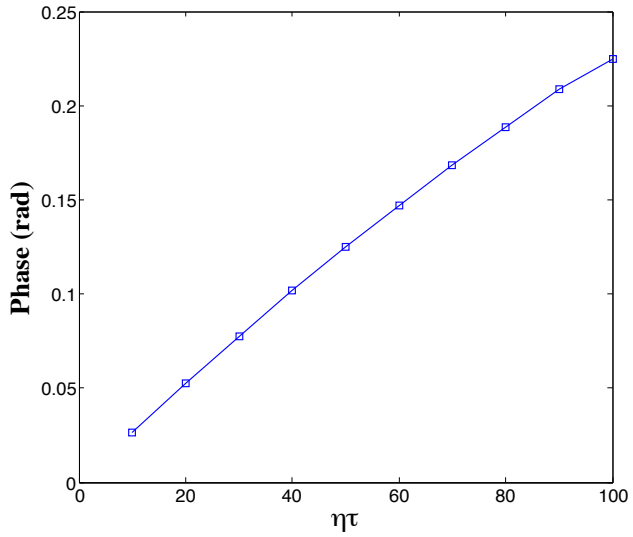

FIG. 5. Numerical results demonstrate a linear increase in the phase shift of the output pulse as a function of the interaction duration τ. The squares '□' correspond to the points calculated numerically, the solid line is the fitting curve obtained and $\eta\tau$ is a dimensionless time parameter.

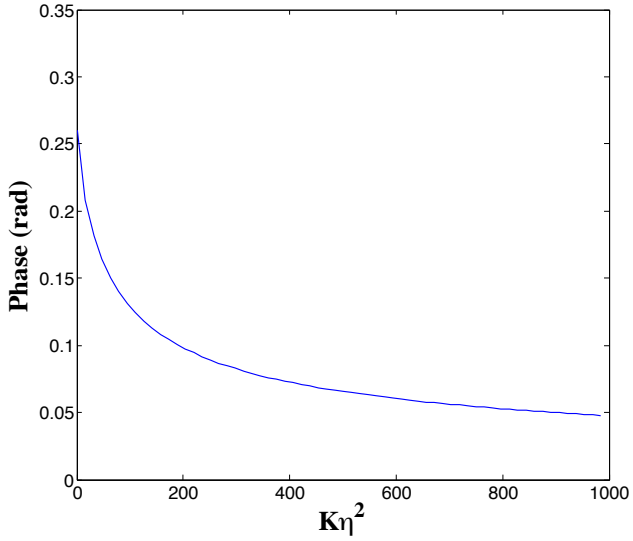

FIG. 6. Numerical results demonstrate that nonlocal interaction range would induce larger phase shift, therefore would perform better compared to the local interactions. Here $K\eta^2$ is a dimensionless parameter which affects the interaction range.

C. Interaction-induced gradient

From the dynamical equations (9) and (11), we can see that the interaction Hamiltonian arises in the equations of motion in the same place as the time-dependent gradient. More explicitly, if we define

$$g_1(\xi,t) = \int_{-\eta}^{\eta} d\xi' \chi(\xi,\xi',t) a_2^\dagger(\xi',t) a_2(\xi',t),$$
$$g_2(\xi,t) = \int_{-\eta}^{\eta} d\xi' \chi(\xi',\xi,t) a_1^\dagger(\xi',t) a_1(\xi',t),$$

then the dynamical equations can be rewritten as

$$\partial_t a_1(\xi,t) = -i(g(\xi,t)+g_1(\xi,t))a_1(\xi,t) - \beta\int_{-\eta}^{\xi} d\xi' a_1(\xi',t) + i\sqrt{\beta} b_{1,in}(t), \quad (14)$$
$$\partial_t a_2(\xi,t) = -i(g(\xi,t)+g_2(\xi,t))a_2(\xi,t) - \beta\int_{-\eta}^{\xi} d\xi' a_2(\xi',t) + i\sqrt{\beta} b_{2,in}(t). \quad (15)$$

From the first term on the right-hand side of equations (14) and (15), we can see that $g_1(\xi,t)$ and $g_2(\xi,t)$ actually appear in the same place in the equation as $g(\xi,t)$.

In certain cases the shape of $g_1(\xi,t)$ and/or $g_2(\xi,t)$ can look very similar to the gradient normally used to read out the excitation stored in the memory, leading to unwanted loss. For example, we plot $g_1(\xi,t)$ and $g_2(\xi,t)$ in Figure 7 for a local interaction with a gaussian-shape pulse for $M1$ and rectangular-shape pulse for $M2$. $g_2(\xi,t)$ happens to be larger in this case, and thus has a stronger effect compared with $g_1(\xi,t)$. If we look at at $g_2(\xi,t)$ past $\xi/\eta = 0$ it looks similar to a downward sloping gradient, much like the gradient used during the readout stage. This results in the excitation past $\xi/\eta = 0$ in $M1$ leaking from the memory. The same also happens to the excitation in $M2$, however the effect is less pronounced as the gradient is less steep. We demonstrate this effect numerically in figures 8 and 9 where the input, output, and stored energy of $M1$ and $M2$, respectively, are plotted (a detailed discussion about the energy balance is in Appendix B.) We found this unwanted loss due to the interaction-induced gradient was common for generic pulse shapes.

There are two ways to ameliorate the effects of an interaction-induced gradient:

1. *Pulse shape engineering* If the waveform of the input pulses are shaped such that the functions $g_1(\xi,t)$ and $g_2(\xi,t)$ are flat, there will be no gradient and thus no additional loss.

2. *Non-local interactions* If the interactions are highly nonlocal, then $g_1(\xi,t)$ and $g_2(\xi,t)$ will be approximately independent of ξ. As $\chi(\xi,\xi',t) \approx 1$ over the region between $-\eta$ and η for very small $K\eta^2$. As $g_1(\xi,t)$ and $g_2(\xi,t)$ will be flat, there will be no loss.

Careful pulse engineering and/or nonlinearity design will be an important part of implementing XPM in practice and will be examined in future work.

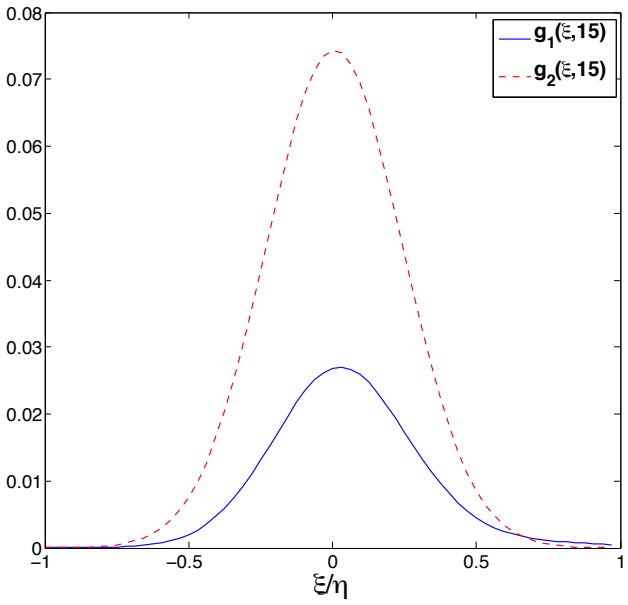

FIG. 7. Plot of effective gradient generated by a square pulse shape $g_1(\xi, t)$ and a gaussian pulse shape $g_2(\xi, t)$. The plot was given for a dimensionless parameter ξ/η denoting the frequence (or spatial position) of the memory at $\eta t = 150$ and $K\eta^2 = 10$.

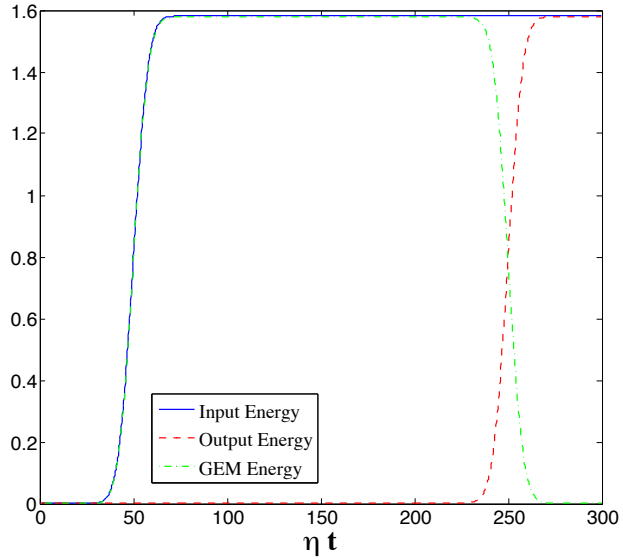

FIG. 8. Input, output and stored energies versus a dimensionless time parameter ηt for GEM1.

IV. CONCLUSIONS

We have presented a theoretical model of interactions in a compound GEM and derived the dynamical equations for the write, interaction and read stages. We have demonstrated the formation of entanglement, XPM and interaction-induced gradients. We applied a Gaussian approximation to numerically simulate its dynamics. The numerical results showed that entanglement could be generated between the two registers. We explored the XPM phenomena, the numerical results demonstrated are in accordance with both theoretical and experimental results in the literature. It was shown that the phase shift of the Gaussian-shape pulse relies quadratically on the strength of the rectangular-shape pulse, and linearly on the interaction duration. Also nonlocal interactions between the registers would perform better than local interactions in the XPM, assuming the maximum interaction strength is the same. For the interaction-induced gradient, we showed that it is an important factor to be considered and careful engineering of the pulse shapes is an important part of implementing XPM. Our model serves as a useful toolbox in the study of photon interactions in a compound GEM and could be used to develop memory-based quantum computing gates.

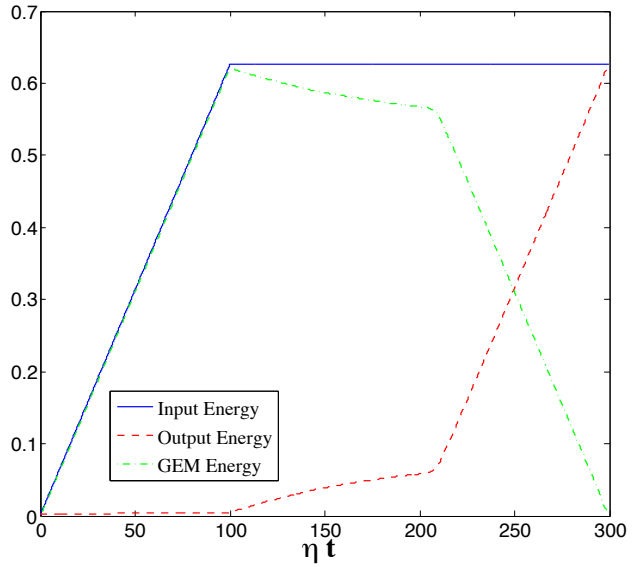

FIG. 9. Input, output and stored energies versus a dimensionless time parameter ηt for GEM2.

ACKNOWLEDGEMENTS

We thank Guodong Shi and Thien Nguyen for useful discussions. We gratefully acknowledge support by the Australian Research Council Centre of Excellence for Quantum Computation and Communication Technology (project number CE110001027), and AFOSR Grant FA2386-12-1-4075).

APPENDIX A. PDES AND GAUSSIAN APPROXIMATIONS

The 8 coupled partial differential equations are given as follows:

$$\partial_t\langle a_1(\xi,t)\rangle = -i\int_{-\eta}^{\eta} d\xi_2\chi(\xi,\xi_2,t)\langle a_1(\xi,t)a_2^\dagger(\xi_2,t)a_2(\xi_2,t)\rangle$$
$$-ig(\xi,t)\langle a_1(\xi,t)\rangle - \beta\langle\int_{-\eta}^{\xi} d\xi' a_1(\xi',t)\rangle\rangle + i\sqrt{\beta}\langle b_{1,\mathrm{in}}(t)\rangle.$$

$$\partial_t\langle a_2(\xi,t)\rangle = -i\int_{-\eta}^{\eta} d\xi_1\chi(\xi_1,\xi,t)\langle a_1^\dagger(\xi_1,t)a_1(\xi_1,t)a_2(\xi,t)\rangle$$
$$-ig(\xi,t)\langle a_2(\xi,t)\rangle - \beta\langle\int_{-\eta}^{\xi} d\xi' a_2(\xi',t)\rangle + i\sqrt{\beta}\langle b_{2,\mathrm{in}}(t)\rangle.$$

$$\begin{aligned}
&\partial_t\langle a_1^\dagger(\xi_1,t)a_1(\xi_2,t)\rangle = \\
&-i\int_{-\eta}^{\eta} d\xi\chi(\xi_2,\xi,t)\langle a_1^\dagger(\xi_1,t)a_1(\xi_2,t)a_2^\dagger(\xi,t)a_2(\xi,t)\rangle \\
&+i\int_{-\eta}^{\eta} d\xi\chi(\xi_1,\xi,t)\langle a_1^\dagger(\xi_1,t)a_1(\xi_2,t)a_2^\dagger(\xi,t)a_2(\xi,t)\rangle \\
&-i\left(g(\xi_2,t)-g(\xi_1,t)\right)\langle a_1^\dagger(\xi_1,t)a_1(\xi_2,t)\rangle \\
&-\beta\langle\int_{-\eta}^{\xi_1} d\xi a_1^\dagger(\xi,t)a_1(\xi_2,t) + \int_{-\eta}^{\xi_2} d\xi a_1^\dagger(\xi_1,t)a_1(\xi,t)\rangle \\
&+i\sqrt{\beta}\langle b_{1,\mathrm{in}}(t)\rangle\langle a_1^\dagger(\xi_1,t)\rangle - i\sqrt{\beta}\langle b_{1,\mathrm{in}}(t)\rangle^*\langle a_1(\xi_2,t)\rangle.
\end{aligned}$$

$$\begin{aligned}
&\partial_t\langle a_2^\dagger(\xi_1,t)a_2(\xi_2,t)\rangle = \\
&-i\int_{-\eta}^{\eta} d\xi\chi(\xi,\xi_2,t)\langle a_1^\dagger(\xi,t)a_1(\xi,t)a_2^\dagger(\xi_1,t)a_2(\xi_2,t)\rangle \\
&+i\int_{-\eta}^{\eta} d\xi\chi(\xi,\xi_1,t)]\langle a_1^\dagger(\xi,t)a_1(\xi,t)a_2^\dagger(\xi_1,t)a_2(\xi_2,t)\rangle \\
&-i\left(g(\xi_2,t)-g(\xi_1,t)\right)\langle a_2^\dagger(\xi_1,t)a_2(\xi_2,t)\rangle \\
&-\beta\langle\int_{-\eta}^{\xi_1} d\xi a_2^\dagger(\xi,t)a_2(\xi_2,t) + \int_{-\eta}^{\xi_2} d\xi a_2^\dagger(\xi_1,t)a_2(\xi,t)\rangle \\
&-i\sqrt{\beta}\langle b_{2,\mathrm{in}}(t)\rangle^*\langle a_2(\xi_2,t)\rangle + i\sqrt{\beta}\langle b_{2,\mathrm{in}}(t)\rangle\langle a_2^\dagger(\xi_1,t)\rangle.
\end{aligned}$$

$$\begin{aligned}
&\partial_t\langle a_1(\xi_1,t)a_1(\xi_2,t)\rangle = \\
&-i\int_{-\eta}^{\eta} d\xi\chi(\xi_2,\xi,t)\langle a_1(\xi_1,t)a_1(\xi_2,t)a_2^\dagger(\xi,t)a_2(\xi,t)\rangle \\
&-i\int_{-\eta}^{\eta} d\xi\chi(\xi_1,\xi,t)\langle a_1(\xi_1,t)a_1(\xi_2,t)a_2^\dagger(\xi,t)a_2(\xi,t)\rangle \\
&-i\left(g(\xi_2,t)+g(\xi_1,t)\right)\langle a_1(\xi_1,t)a_1(\xi_2,t)\rangle \\
&-\beta\langle\int_{-\eta}^{\xi_1} d\xi a_1(\xi,t)a_1(\xi_2,t) + \int_{-\eta}^{\xi_2} d\xi a_1(\xi,t)a_1(\xi_1,t)\rangle \\
&+i\sqrt{\beta}\langle b_{1,\mathrm{in}}(t)\rangle\langle a_1(\xi_1,t)\rangle + i\sqrt{\beta}\langle b_{1,\mathrm{in}}(t)\rangle\langle a_1(\xi_2,t)\rangle.
\end{aligned}$$

$$\begin{aligned}
&\partial_t\langle a_2(\xi_1,t)a_2(\xi_2,t)\rangle = \\
&-i\int_{-\eta}^{\eta} d\xi\chi(\xi,\xi_2,t)\langle a_1^\dagger(\xi,t)a_1(\xi,t)a_2(\xi_1,t)a_2(\xi_2,t)\rangle \\
&-i\int_{-\eta}^{\eta} d\xi\chi(\xi,\xi_1,t)\langle a_1^\dagger(\xi,t)a_1(\xi,t)a_2(\xi_1,t)a_2(\xi_2,t)\rangle \\
&-i\left(g(\xi_2,t)+g(\xi_1,t)\right)\langle a_2(\xi_1,t)a_2(\xi_2,t)\rangle \\
&-\beta\langle\int_{-\eta}^{\xi_1} d\xi a_2(\xi,t)a_2(\xi_2,t) + \int_{-\eta}^{\xi_2} d\xi a_2(\xi,t)a_2(\xi_1,t)\rangle \\
&+i\sqrt{\beta}\langle b_{2,\mathrm{in}}(t)\rangle\langle a_2(\xi_1,t)\rangle + i\sqrt{\beta}\langle b_{2,\mathrm{in}}(t)\rangle\langle a_2(\xi_2,t)\rangle.
\end{aligned}$$

$$\begin{aligned}
&\partial_t\langle a_1(\xi_1,t)a_2(\xi_2,t)\rangle = \\
&-i\int_{-\eta}^{\eta} d\xi\chi(\xi,\xi_2,t)\langle a_1^\dagger(\xi,t)a_1(\xi,t)a_1(\xi_1,t)a_2(\xi_2,t)\rangle \\
&-i\int_{-\eta}^{\eta} d\xi\chi(\xi_1,\xi,t)\langle a_2^\dagger(\xi,t)a_2(\xi,t)a_1(\xi_1,t)a_2(\xi_2,t)\rangle \\
&-i\chi(\xi_1,\xi_2,t)\langle a_1(\xi_1,t)a_2(\xi_2,t)\rangle \\
&-i\left(g(\xi_2,t)+g(\xi_1,t)\right)\langle a_1(\xi_1,t)a_2(\xi_2,t)\rangle \\
&-\beta\langle\int_{-\eta}^{\xi_1} d\xi a_1(\xi,t)a_2(\xi_2,t) + \int_{-\eta}^{\xi_2} d\xi a_1(\xi_1,t)a_2(\xi,t)\rangle \\
&+i\sqrt{\beta}\langle b_{1,\mathrm{in}}(t)\rangle\langle a_2(\xi_2,t)\rangle + i\sqrt{\beta}\langle b_{2,\mathrm{in}}(t)\rangle\langle a_1(\xi_1,t)\rangle.
\end{aligned}$$

$$\begin{aligned}
&\partial_t\langle a_1(\xi_1,t)a_2^\dagger(\xi_2,t)\rangle = \\
&i\int_{-\eta}^{\eta} d\xi\chi(\xi,\xi_2,t)\langle a_1^\dagger(\xi,t)a_1(\xi,t)a_1(\xi_1,t)a_2^\dagger(\xi_2,t)\rangle \\
&-i\int_{-\eta}^{\eta} d\xi\chi(\xi_1,\xi,t)\langle a_2^\dagger(\xi,t)a_2(\xi,t)a_1(\xi_1,t)a_2^\dagger(\xi_2,t)\rangle \\
&+i\chi(\xi_1,\xi_2,t)\langle a_1(\xi_1,t)a_2^\dagger(\xi_2,t)\rangle \\
&-i\left(g(\xi_1,t)-g(\xi_2,t)\right)\langle a_1(\xi_1,t)a_2^\dagger(\xi_2,t)\rangle \\
&-\beta\langle\int_{-\eta}^{\xi_1} d\xi a_1(\xi,t)a_2^\dagger(\xi_2,t) + \int_{-\eta}^{\xi_2} d\xi a_1(\xi_1,t)a_2^\dagger(\xi,t)\rangle \\
&+i\sqrt{\beta}\langle b_{1,\mathrm{in}}(t)\rangle\langle a_2^\dagger(\xi_2,t)\rangle - i\sqrt{\beta}\langle b_{2,\mathrm{in}}(t)\rangle^*\langle a_1(\xi_1,t)\rangle.
\end{aligned}$$

We approximate the third-order terms and fourth-order terms in the above PDEs using first-order and second-order expressions employing Gaussian approximations, which is termed as *Isserlis' theorem* in probability theory [24, 25]. More explicitly, the approximation equations are given below:

$$\begin{aligned}
\langle O_1O_2O_3\rangle \approx\ &\langle O_1O_2\rangle\langle O_3\rangle + \langle O_1O_3\rangle\langle O_2\rangle \\
&+\langle O_2O_3\rangle\langle O_1\rangle - 2\langle O_1\rangle\langle O_2\rangle\langle O_3\rangle, \\
\langle O_1O_2O_3O_4\rangle \approx\ &\langle O_1O_2\rangle\langle O_3O_4\rangle + \langle O_1O_3\rangle\langle O_2O_4\rangle \\
&+\langle O_1O_4\rangle\langle O_2O_3\rangle - 2\langle O_1\rangle\langle O_2\rangle\langle O_3\rangle\langle O_4\rangle.
\end{aligned}$$

Here O_i can be either the annihilation operator or the creation operator.

APPENDIX B. ENERGY BALANCE

Here, we show that the energy is balanced for $M1$ and $M2$ in the XPM model.

Recall that for the memory model in [15], the energy balance equation is stated as below:

$$\int_0^t d\tau b_{\rm in}^\dagger(\tau) b_{\rm in}(\tau) = \int_0^t d\tau b_{\rm out}^\dagger(\tau) b_{\rm out}(\tau) + \int_{-\eta}^{\eta} d\xi a^\dagger(\xi,t) a(\xi,t).$$

For the XPM model, the energy balance equation for $M1$ can be stated as below:

$$\int_0^t d\tau b_{1,\rm in}^\dagger(\tau) b_{1,\rm in}(\tau) = \int_0^t d\tau b_{1,\rm out}^\dagger(\tau) b_{1,\rm out}(\tau) + \int_{-\eta}^{\eta} d\xi a_1^\dagger(\xi,t) a_1(\xi,t), \tag{A16}$$

which is equivalent to the following one:

$$b_{1,\rm in}^\dagger(t) b_{1,\rm in}(t) = b_{1,\rm out}^\dagger(t) b_{1,\rm out}(t) + \int_{-\eta}^{\eta} d\xi \frac{\partial a_1^\dagger(\xi,t) a_1(\xi,t)}{\partial t}.$$

From the input-output equation (10)

$$b_{1,\rm out}(t) = i\sqrt{\beta}\int_{-\eta}^{\eta} d\xi a_1(\xi,t) + b_{1,\rm in}(t)$$

and the dynamical equation for $a_1^\dagger(\xi,t)a_1(\xi,t)$ which can be derived as below

$$\begin{aligned}&\frac{\partial a_1^\dagger(\xi,t)a_1(\xi,t)}{\partial t}\\ &= -\beta\int_{-\eta}^{\xi} d\xi' a_1^\dagger(\xi,t)a_1(\xi',t) - \beta\int_{-\eta}^{\xi} d\xi' a_1^\dagger(\xi',t)a_1(\xi,t)\\ &\quad -i\sqrt{\beta}b_{1,\rm in}^\dagger(t)a_1(\xi,t) + i\sqrt{\beta}a_1^\dagger(\xi,t)b_{1,\rm in}(t),\end{aligned}$$

we can easily derive equation (A16). The above proof goes along similarly for $M2$, therefore for the XPM model, the energy is balanced, also there is no energy flow between $M1$ and $M2$.

REFERENCES

[1] Yoran, N. and Reznik, B., Deterministic linear optics quantum computation with single photon qubits. *Physical review letters, 91(3), 037903,(2003).*

[2] Knill, E., Laflamme, R., and Milburn, G. J. , A scheme for efficient quantum computation with linear optics. *Nature, 409(6816), 46-52, (2001).*

[3] Milburn, G. J. Quantum optical Fredkin gate. *Physical Review Letters, 62(18), 2124,(1989).*

[4] Kok, P., Munro, W. J., Nemoto, K., Ralph, T. C., Dowling, J. P. and Milburn, G. J. Linear optical quantum computing with photonic qubits. *Reviews of Modern Physics, 79(1), 135, (2007).*

[5] Chuang, I. L. and Yamamoto, Y., Simple quantum computer. *Physical review. A, 52(5), 3489, (1995).*

[6] Matsuda, N., Shimizu, R., Mitsumori, Y., Kosaka, H. and Edamatsu, K., Observation of optical-fibre Kerr nonlinearity at the single-photon level. *Nature photonics, 3(2), 95-98, (2009).*

[7] Schmidt, H. and Imamoglu, A., Giant Kerr nonlinearities obtained by electromagnetically induced transparency. *Optics letters, 21(23), 1936-1938, (1996).*

[8] Shapiro, J. H., Single-photon Kerr nonlinearities do not help quantum computation. *Physical Review A, 73(6), 062305, (2006).*

[9] Shen, J. T. and Fan, S. Strongly correlated two-photon transport in a one-dimensional waveguide coupled to a two-level system. *Physical review letters, 98(15), 153003, (2007).*

[10] Gea-Banacloche, J., Impossibility of large phase shifts via the giant Kerr effect with single-photon wave packets. *Physical Review A, 81(4), 043823, (2010).*

[11] Xu, S., Rephaeli, E. and Fan, S. Analytic properties of two-photon scattering matrix in integrated quantum systems determined by the cluster decomposition principle. *Physical review letters, 111(22), 223602,(2013).*

[12] Hétet, G., Longdell, J. J., Alexander, A. L., Lam, P. K. and Sellars, M. J., Electro-optic quantum memory for light using two-level atoms. *Physical review letters, 100(2), 023601,(2008).*

[13] Hosseini, M., Rebić, S., Sparkes, B. M., Twamley, J., Buchler, B. C. and Lam, P. K., Memory-enhanced noiseless cross-phase modulation. *Light: Science & Applications , 1(12), e40, (2012).*

[14] Hosseini, M., Sparkes, B. M., Campbell, G., Lam, P. K., and Buchler, B. C., High efficiency coherent optical memory with warm rubidium vapour. *Nature communications, 2, 174, (2011).*

[15] Hush, M. R., Carvalho, A. R. R., Hedges, M., and James, M. R., Analysis of the operation of gradient echo memories using a quantum input-output model. *New Journal of Physics, 15(8), 085020, (2013).*

[16] Gardiner, C. and Zoller, P., Quantum noise: a handbook of Markovian and non-Markovian quantum stochastic methods with applications to quantum optics (Vol. 56). *Springer Science & Business Media, (2004).*

[17] Gough, J. and James, M. R., The series product and its application to quantum feedforward and feedback networks. *Automatic Control, IEEE Transactions on,*

54(11), 2530-2544, (2009).

[18] Dennis, G. R., Hope, J. J. and Johnsson, M. T., XMDS2: Fast, scalable simulation of coupled stochastic partial differential equations. *Computer Physics Communications, 184(1), 201-208, (2013).*

[19] Chen, Y. F., Wang, C. Y., Wang, S. H. and Ite, A. Y. , Low-light-level cross-phase-modulation based on stored light pulses. *Physical review letters, 96(4), 043603,(2006).*

[20] Giedke, G., and Cirac, J. I., Characterization of Gaussian operations and distillation of Gaussian states. *Physical Review A, 66(3), 032316. (2002).*

[21] Życzkowski, K., Horodecki, P., Sanpera, A., and Lewenstein, M. Volume of the set of separable states. *Physical Review A, 58(2), 883.(1998).*

[22] Eisert, J., Entanglement in quantum information theory. *arXiv preprint quant-ph/0610253. (2006).*

[23] Vidal, G., and Werner, R. F., Computable measure of entanglement. *Physical Review A, 65(3), 032314. (2002).*

[24] Isserlis, L. , On certain probable errors and correlation coefficients of multiple frequency distributions with skew regression. *Biometrika, 185-190. (1916).*

[25] Isserlis, L. , On a formula for the product-moment coefficient of any order of a normal frequency distribution in any number of variables. *Biometrika, 134-139.(1918).*

[26] Henkel, N. and Nath, R. and Pohl, T. , Three-Dimensional Roton Excitations and Supersolid Formation in Rydberg-Excited Bose-Einstein Condensates. *Physical review letters, 104(19), 195302, (2010)*